THE JOURNAL OF PHYSICAL CHEMISTRY B

Article

pubs.acs.org/JPCB

Important Role of Surface Fluoride in Nitrogen-Doped TiO_2 Nanoparticles with Visible Light Photocatalytic Activity

Jonathan I. Brauer† and Greg Szulczewski*

Department of Chemistry, The University of Alabama, Tuscaloosa, Alabama 35487, United States

ABSTRACT: Nitrogen-doped TiO_2 nanoparticles have been synthesized using sol−gel methods and subsequently fluorinated at room temperature by aging in acidic solutions of NaF. The nanoparticles were characterized by X-ray photoelectron spectroscopy, X-ray diffraction, UV−vis, and IR diffuse reflectance spectroscopy. After aging at room temperature in NaF solutions, the Ti−OH groups on the surface of the TiO_2 nanoparticles were replaced by Ti−F bonds, which resulted in a decrease of the point of zero charge from pH 5.4 to 2.8. Most importantly, the nitrogen dopants were retained after the fluorination process, and the amorphous nanoparticles were partially converted into the anatase phase. Annealing the photocatalysts resulted in a decrease of both the nitrogen and fluoride atomic concentration. Diffuse reflectance spectra show an increase in absorbance above 400 nm after annealing the F,N-doped TiO_2, which suggests the formation of color centers. The photoactivity of the F,N-doped and N-doped TiO_2 catalysts were evaluated by monitoring by the decolorization of methylene blue with visible light. Mass spectrometric analysis revealed that methylene blue undergoes successive demethylation, and more importantly, the rate of decolorization depends on the fluoride concentration. These results show the importance of a two-step synthesis method to independently control the nitrogen and fluoride concentration.

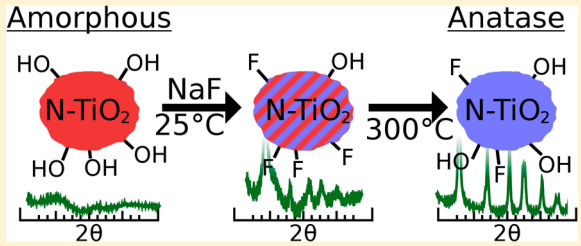

INTRODUCTION

The quest to synthesize nanoscale photocatalysts that display high activity with visible light to decompose organic pollutants or catalyze water splitting is very important to future environmental and energy technologies.[1−3] In particular, TiO_2 has been studied more than any other material owing to its chemical stability, nontoxicity, and abundance. However, pure TiO_2 is only photoactive with ultraviolet radiation, since its optical gap is approximately 3.2 eV. There are many reports to lower the band gap by chemical doping, either by inorganic metal ions or nonmetals.[4−8] Perhaps the first report of nitrogen doping was published in 1985 by Sato.[9] However, it was the work of Asahi et al. in 2001 that catalyzed an enormous effort to dope TiO_2 with p-block elements in order to realize visible light photocatalytic activity.[10] A critical evaluation of this literature reveals a great variability in the efficiency of TiO_2 photocatalysts because many variables influence the performance. For example, the photocatalytic activity has been shown to depend on the morphology, phase, surface area, surface charge, and even the substrate used to measure photoactivity.[11]

Sol−gel synthesis of titania nanomaterials is well-established chemistry.[12] There have been many reports to control both the morphology and phase of titania using hydrothermal methods.[13−16] In the case of nitrogen doping, the general strategy is to include a nitrogen-containing precursor in the synthesis. Many different organic and inorganic amines have been used, for example, ammonia, urea, triethylamine, ammonium chloride, etc. The organic amines tend to decompose and leave hydrocarbon fragments in the lattice. In fact, many of the early reports of N-doped TiO_2 contained significant amounts of carbon impurities, as revealed through IR spectroscopy.[17−20] Ammonium chloride has proven to be an effective nitrogen source because is does not contain any carbon. Despite the differences in sample preparation and nitrogen precursor selection, some general conclusions can be drawn about the composition and photoactivity of N-TiO_2. First, the presence of localized states within the band gap is considered to be responsible for the absorption of visible light in N-doped TiO_2. In principle, nitrogen can replace oxygen in the lattice (i.e., substitutional) or form interstitial species. Density functional theory calculations indicate that both types of nitrogen species introduce localized states in the band gap, but the interstitial nitrogen states occur at slightly higher energy.[21] Experimentally, the substitutional species can be readily identified by X-ray photoelectron spectroscopy (XPS). It is generally accepted that the substitutional nitrogen in TiO_2 has a binding energy near 397 eV.[22−25] The interstitial species are much more difficult to identify by XPS, but most sol−gel methods produce a nitrogen species with a binding energy near 400 ± 1 eV.[26−31] Electron paramagnetic resonance (EPR) spectroscopy has revealed significant insight into the nature of the photoactive species in N-TiO_2.[32−37] The paramagnetic species observed in EPR is generally written as NO^{2-}. The other interstital site is diamagnetic (labeled as NO^{3-}) and EPR silent. Upon excitation with visible light greater than 420 nm, both the paramagnetic and diamagnetic centers are capable of

Special Issue: Spectroscopy of Nano- and Biomaterials Symposium

Received: July 16, 2014
Revised: September 10, 2014

   dx.doi.org/10.1021/jp5071049 | J. Phys. Chem. B XXXX, XXX, XXX−XXX

generating reactive electrons in the valence band and holes in the conduction band.[36] However, action spectra reveal the photoefficiency is very low when the wavelength exceeds 450 nm.[38]

The effect of fluoride ion adsorption and its subsequent role in UV light driven photocatalytic process has been intensively studied in TiO_2 nanoparticles.[39−50] One of the first comprehensive studies was reported in 2000 by Minero et al.[39,40] They calculated the surface coverage of Ti−F sites as a function of solution pH and fluoride ion concentration. The model predicts the maximum number of Ti−F sites exists near pH ∼3. They found the rate of photocatalytic degradation of phenol was four times higher (than unmodified Degussa P25) when the fluorination was done with 10 mM NaF at pH ∼ 4. In 2004, Park and Choi studied the effect of TiO_2 surface fluorination using photoelectrochemistry.[44] They found that short-circuit photocurrents were decreased after fluorination of a TiO_2/Pt electrode, which they attributed to the Ti−F group acting as an electron-trapping site. In 2005, the enhanced production of hydroxyl radicals due to fluorination of P25 was observed by Mrowetz and Selli.[51] Using the spin-trap DMPO, they measured an increased concentration of the DMPO−OH adduct as a function of irradiation time. Furthermore, they observed that the addition of 2-propanol, a known hydroxyl scavenger, decreased the rate of decolorization of the acid Red dye molecule. Taken together, these results showed an enhanced rate of UV light-induced production of hydroxyl radicals on fluorinated TiO_2 to degrade model pollutants.

Prior studies have shown a synergistic benefit of both fluoride and nitrogen doping of TiO_2 photocatalysts.[37,38,52−62] In general, both a nitrogen and fluorine precursor are added during the sol−gel synthesis. In some cases, ammonia fluoride was used as both the nitrogen and fluorine source. Interestingly, some synthesis conditions produce surface fluoride (i.e., Ti−F) and/or bulk fluoride (i.e., Ti−F−Ti). These two species are readily differentiated by XPS. The binding energy of the surface fluoride is ∼685 eV, while the lattice-bound fluoride has a binding energy of ∼688 eV. Here we report a synthetic strategy that allows the incorporation of nitrogen dopants into an amorphous TiO_2 structure, followed by a second step that forms nanoparticles with the anatase phase and adsorbed fluoride at room temperature. This two-step procedure allows for independent control of the dopant concentration, surface chemistry, and morphology at room temperature. Consequently, the focus of this study is to characterize the surface of these nanoparticles synthesized under different solution pH and annealing temperatures to determine the relative amount of nitrogen and fluoride. A secondary objective was to correlate the nitrogen and fluoride composition to the visible light induced photocatalytic activity.

EXPERIMENTAL SECTION

A titanium precursor solution was made by mixing 15 mL of titanium isopropoxide (97%, Aldrich) with 10 mL of 2-propanol (HPLC-grade, Aldrich) in an addition funnel. In a three-neck flask 100 mL of purified water (18.3 MΩ cm, Barnstead EASYpure LF) was mixed with 0.2 mL of 1.0 M hydrochloric acid (Aldrich) to adjust the pH to below 3. The three-neck flask was placed in an ice bath and cooled to 2 °C. Dropwise (∼1 drop/2 s) addition of the titanium precursor to the chilled water (under vigorous stirring) produced a milky solution of suspended TiO_2 nanoparticles. The solid product was collected by centrifugation at 3000 rpm for 10 min. The supernatant was discarded, and the product was resuspended in water. Five centrifugation wash cycles were repeated to ensure that any residual 2-propanal or HCl was removed. The resulting solid was then dried in a vacuum chamber (pressure of 10^{-2} Torr) at room temperature overnight. The final dried powder is referred to below as "as synthesized". Nitrogen-doped samples were prepared by the same method but with the inclusion of 8 g of NH_4Cl in the chilled water. The same purification scheme was used as described above. The as-synthesized powders were "aged" in polypropylene containers by adding ∼300 mg of TiO_2 nanoparticles in a 100 mL aqueous NaF solution. The concentration of the NaF solutions varied from 10 to 100 mM, and the pH varied from about 2 to 7 (by addition of 0.1 M HCl). The suspension was vigorously stirred for 24 h then washed with deionized water and centrifuged (by the same method above) until the free fluoride ion concentration dropped below the detection limit of the ion-selective electrode. Samples were annealed at 100, 200, 300, and 400 °C in a tube furnace in air for 6 h after increasing the temperature at a rate of 5 °C/min.

The samples were characterized by X-ray diffraction (XRD), UV−vis diffuse-reflectance spectroscopy (DRS), diffuse infrared reflection spectroscopy (DRIFTS), and XPS. The XRD measurements were done on a Bruker D2 Phaser desktop diffractometer with a Cu Kα X-rays. The DRS measurements were done with a Shimadzu UV-3600 UV−vis equipped with a Harrick Scientific Praying Mantis Diffuse Reflection Accessory. The spectra were normalized relative to a Teflon standard. The XPS measurements were done with a Kratos Axis 165 spectrometer using a monochromatic Al Kα X-ray. Samples were prepared for XPS measurements by suspending the particles in an acidic solution to minimize particle aggregation then drop casting onto a gold-coated Si wafer. No charging was observed, and the binding energy scale was set so that the adventitious C(1s) peak was 285.0 eV. XPS measurements were performed with the spectrometer pass energy set to 80 eV, and the monochromatic Al Kα X-ray source was operated at 150 W.

A fluoride ion selective electrode attached to a Orion Research Expandable Ion Analyzer EA940 was used to measure the fluoride ion concentration in solution. All measurements were done in a total ionic strength adjustment buffer. The pH at the point of zero charge (pH_{pzc}) was measured by the common intersection point method.[63] A suspension of 180 mg of TiO_2 powder in 9 mL of purified water (2% w/w) was prepared and split into three aliquots. To each aliquot, enough NaCl was added to bring the concentration of each solution to 0.1, 0.01, and 0.001 M, respectively. Aliquots were then titrated with 0.01 M HCl (also containing the NaCl solution of the same concentration); the pH was recorded after each addition. This was repeated with 0.01 M NaOH and plotted. Since the measured pH will not be affected at the point of zero surface charge, the pH where the titration curves intersect is reported as the pH_{pzc}.

The photocatalytic activity was determined by measuring the rate of methylene blue decolorization. Typically about 5−10 mg of the nanoparticles were added to 40 mL of water in a quartz cuvette. The solution was stirred in the dark for several hours to ensure equilibration. The samples were exposed to radiation between 400 and 560 nm by using a combination of cutoff filters and a water cell to remove ultraviolet and infrared radiation from a 300 W Xe lamp. During irradiation, the samples were magnetically stirred and open to the lab atmosphere. After a period of irradiation, an aliquot was

dx.doi.org/10.1021/jp5071049 | J. Phys. Chem. B XXXX, XXX, XXX−XXX

removed, and the particles were separated from the solution by centrifugation. The optical absorbance of particle-free solution was measured with a Beckman Coulter DU800 UV−vis spectrophotometer. On some aliquots, mass spectra were obtained with a Bruker HCTUltra PTM discovery system using an electrospray ion source. In each experiment, 100 μL of the irradiated solution (particle free) was removed from the reaction cuvette and added to 400 μL of purified water in a 1.5 mL microcentrifuge tube. The solutions were centrifuged at 7000 rpm for 20 min to separate the nanoparticles, and a 250 μL aliquot was drawn for sampling. The sample line and electrospray needle were flushed with 100 μL of the sample before data was collected. The injection speed was 150−400 μL/hour, and the final result was a 60 s average. The source was set to 5 nA, and the N_2 nebulizer gas pressure was set to 10 psi (or 5 L/min) at 250 °C.

RESULTS AND DISCUSSION

Figure 1 shows high-resolution X-ray photoelectron spectra of the as-synthesized N−TiO_2 sample. The N(1s) region can be fit to two peaks: one centered at 401.4 eV and another at 400.0 eV. From the integrated area of the two N(1s) and Ti(2p) peaks and sensitivity factors for the Kratos spectrometer, we calculated an N/Ti atomic ratio of 0.0568 for the as-synthesized particles. The binding energy of the Ti($2p_{3/2}$) peak was centered at 459.1 eV, which is indicative of Ti^{4+}. The O(1s) spectrum has a main peak at 532 eV and a small shoulder near 534 eV that is due to surface titanol groups (Ti−O−H). The assignment of the N(1s) peak has been the subject of much debate.[26−31] There are a few key points we wish to make here before attempting to assign the identity of the nitrogen species. First, there are large differences in the synthesis methods. Many nanoparticles are synthesized by a solution chemical reaction, followed by thermal annealing. In contrast, there are physical methods such as ion implantation, sputtering, and plasma-assisted vapor deposition. These latter methods are highly nonthermal and typically produce substitutional nitrogen. Second, due to the low concentration of nitrogen, typically less than 5 atomic percent with respect to titanium, the signal-to-noise is low. Furthermore, the absolute binding energies are often referenced to the C(1s) level. A survey of the literature shows that most papers set the C(1s) between 285.0 and 284.5 eV. In addition, the spectral resolution is dependent on the pass energy of the analyzer, and the depth of analysis is dependent on the takeoff angle. Finally, some of the samples were lightly etched with Ar ions to remove adventitious contamination before analysis. Collectively, these differences make comparison of results very challenging. With these caveats in mind, we

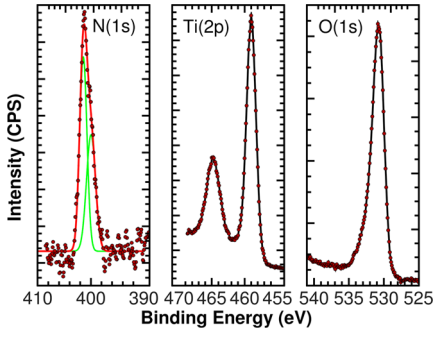

Figure 1. X-ray photoelectron spectra of the as-synthesized N-TiO_2.

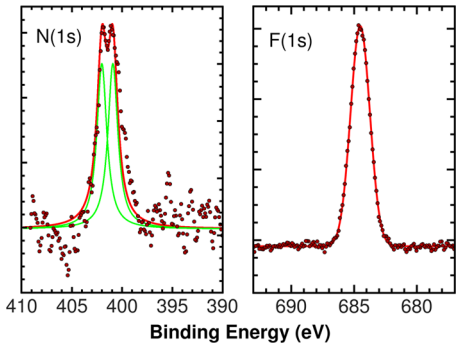

Figure 2. X-ray photoelectron spectra after fluorination.

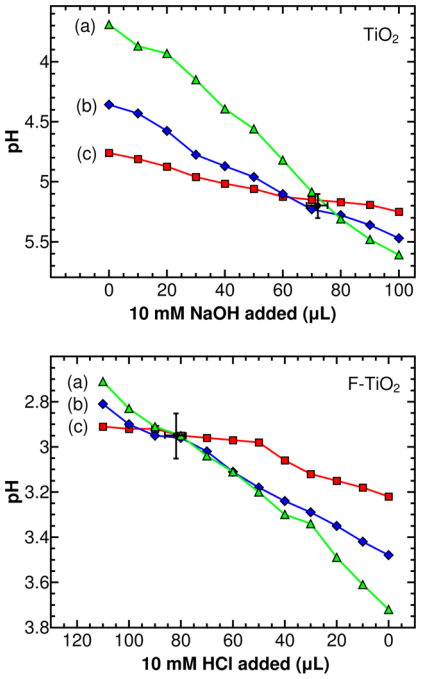

Figure 3. Determination of the point of zero charge for the as-synthesized TiO_2 and fluorinated TiO_2 particles.

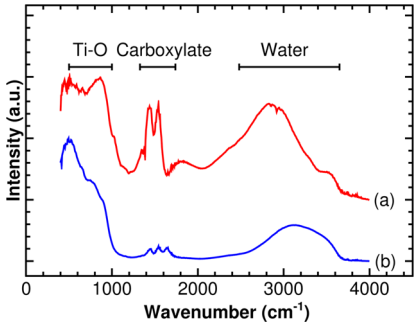

Figure 4. Diffuse reflection IR spectroscopy of the (a) as-synthesized N-TiO_2 and (b) after fluorination in 100 mM NaF.

begin with establishing the expected trend for N(1s) binding energies based on initial state effects.[64] Previous work has established a 1.3 eV shift in the binding energy per oxidation state on nitrogen.[64] For example, metal nitrides are typically found near 397 eV, where the charge on nitrogen is −3. On the other extreme, when nitrogen is oxidized, as in the case of NO_3^- and NO_2^-, the binding energies are 407.4 and 403.6 eV, respectively.[64] As a result, the binding energy of a N^+ and N^0

dx.doi.org/10.1021/jp5071049 | J. Phys. Chem. B XXXX, XXX, XXX−XXX

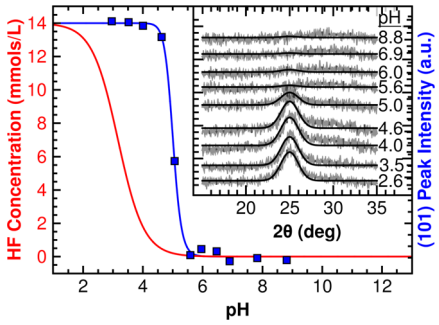

Figure 5. Intensity of the (101) Bragg peak as a function of solution pH (the blue line is a guide for the eye). The calculated equilibrium concentration of HF is shown as the red line.

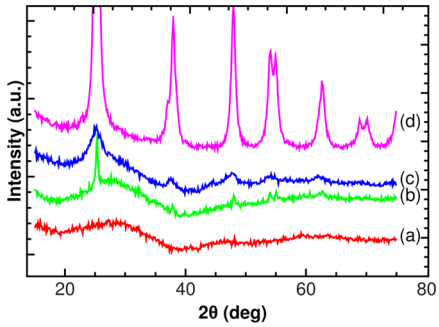

Figure 6. X-ray diffraction of (a) as-synthesized N-TiO_2, (b) N-TiO_2 annealed to 300 °C, (c) N-TiO_2 fluorinated in NaF, and (d) annealing F,N-TiO_2 particles to 300 °C.

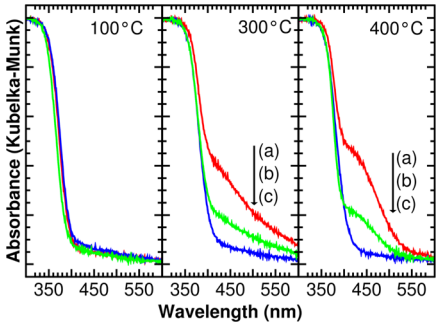

Figure 7. Diffuse-reflection spectroscopy of annealed nanoparticles (a) N-TiO_2, (b) F,N-TiO_2 (pH = 7), and (c) F,N-TiO_2 (pH = 3).

Table 1. Summary of the Atomic Composition of Photocatalysts after Annealing

sample		N/Ti ratio (%)	F/Ti ratio (%)
N-doped TiO_2	unannealed	5.68	–
	100 °C	4.88	–
	200 °C	4.04	–
	300 °C	2.08	–
	400 °C	2.05	–
F,N-doped TiO_2	Unannealed	7.16	55.4
	100 °C	4.61	55.0
	200 °C	3.08	41.1
	300 °C	1.88	16.0
	400 °C	2.39	8.3

center are expected to be near 401.3 and 400 eV, respectively. We tentatively assign the peak at 401.4 eV to adventitious NH_4^+ adsorbed to the surface and the peak at 400.0 eV to an

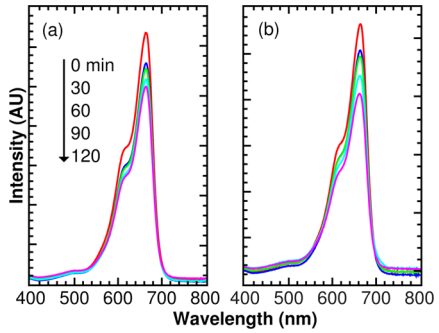

Figure 8. UV–vis spectra of methylene blue following irradiation in (a) N-TiO_2 and (b) F,N-TiO_2 particles.

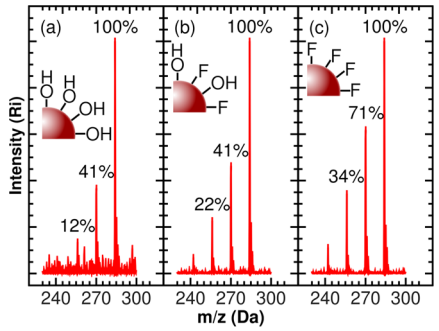

Figure 9. ESI-MS after irradiation of (a) N-TiO_2, (b) F,N-TiO_2 (pH = 7), and (c) F,N-TiO_2 (pH = 3) for 210 min.

"interstitial" nitrogen center. The justification for the assignment is based (in part) on the fact that the high binding energy peaks decrease upon fluorination (see below). Also, the peak at 400 eV has been observed in several reports when NH_4Cl was used as the nitrogen source.[31,32] We did not find evidence for a substitutional nitrogen peak at ~397 eV in any of our as-synthesized or annealed samples (see below). In Figure 2, the presence of fluorine is confirmed after aging in NaF solutions. The F(1s) peak observed at 684.5 eV is characteristic of a surface fluoride species.[31,38,44,59] The relative intensity of the 401.4 eV peak decreases with respect to the 400.0 eV peak after fluorination. After annealing, the F(1s) peak decreased in intensity without a shift in binding energy (see below). Also, we never observed a peak near 688 eV, which would indicate bulk doping of TiO_2.[41]

Figure 3 shows the data from the common intersection point method to determine the point of zero surface charge for the as-synthesized and fluorinated TiO_2. The titrations suggest the pH_{pzc} is near 5.4 for the as-synthesized TiO_2. After fluorination, the pH_{pzc} dropped to about 2.9. At pH values below (above) the pzc, the nanoparticles are positively (negatively) charged. The decrease in pzc is consistent with other literature reports that show surface fluorination lowers the pzc as Ti–O–H groups are replaced with Ti–F bonds.[65] The surface charge is an important parameter because it strongly influences the adsorption process. In our studies, the pH of the irradiated solutions was about 8, so the particles are negatively charged. Since methylene blue is a cationic dye, there is a strong electrostatic attraction to the particles. Further details about the surface groups can be inferred from IR spectroscopy of dried samples. Figure 4 shows DRIFTS spectra before and after NaF treatment. The main difference between the two samples is the intensity of the peaks between 1200 and 1500 cm^{-1}. The as-

dx.doi.org/10.1021/jp5071049 | J. Phys. Chem. B XXXX, XXX, XXX–XXX

synthesized N−TiO_2 shows peaks at 1350, 1450, and 1550 cm^{-1}. These modes can be assigned to a bicarbonate species that resulted from the reaction of atmospheric carbon dioxide with the hydroxylated surface.[66,67] After fluorination, all three peaks decreased in intensity. There is a small peak at 1650 cm^{-1} that can be assigned to the bending mode of physisorbed water. The very broad band from 2000 to 3500 cm^{-1} is due to the O−H stretching mode of physisorbed water molecules in an extensive network of hydrogen bonding.[68] In both samples, the high-energy shoulder near 3600 cm^{-1} is due to linear and/or bridging hydroxyl groups bonding directly to titanium.[69]

The effect of fluorination on the phase of the nanoparticles was studied by XRD. Figure 5 shows the intensity of the (101) Bragg peak as a function of the NaF solution pH. There is a clear dependence on the intensity of the (101) peak as a function of solution pH. Above pH 5, the anatase phase does not form, which coincides with an increase in the equilibrium HF concentration. The anatase phase of TiO_2 is known to be soluble in HF, while the rutile phase is not.[70] The pH also has a large effect on the amount of adsorbed fluoride. Calculations and experiments show that the maximum amount of fluoride occurs near pH ∼ 3, and almost no fluoride adsorbs above pH ∼ 8.[39,44] For example, in the case of P25, Park and Choi calculated that 98.5% of the fluoride ion in a 10 mM solution of NaF should adsorb at pH = 3 while only 12.5% adsorbs at pH = 7.[44] Figure 6 shows XRD spectra for the various TiO_2 samples. In spectrum (a) the as-synthesized N−TiO_2 powder does not show any strong Bragg reflections. After annealing the as-synthesized sample in air for 6 h at 300 °C, there is a weak diffraction peak observed at ∼24 ° as shown in (b). After the as-synthesized N−TiO_2 was aged in a NaF solution (pH ∼3) for 24 h (and dried), the appearance of weak Bragg peaks due to formation of the anatase phase is shown in (c). Finally, when the fluorinated sample was annealed in air at 300 °C for 6 h, the appearance of well-defined Bragg peaks corresponding to the anatase phase is shown in (d). The main anatase peaks are observed at 25.3, 38.0, 48.0, 54.1, 55.0, 62.7, 68.9, and 70.2°, corresponding to the (101), (004), (200), (105), (211), (204), (116), and (220) planes, respectively. No other peaks corresponding to the rutile or brookite phase were observed. With the use of the Scherrer equation and the fwhm of the (101) peak, the crystallite size after annealing is estimated to be about 10−20 nm. Previous work has shown that adsorbed fluoride is known to inhibit particle sintering.[71]

In Figure 7, a set of DRS spectra for (a) as-synthesized TiO_2, (b) partially fluorinated N−TiO_2, and (c) fully fluorinated N−TiO_2 nanoparticles are shown as a function of annealing temperature. Interestingly, all of the unannealed particles have virtually the same reflectance spectrum. However, upon annealing, several changes occur. First, both the nitrogen and fluorine signals decrease. Table 1 summarizes the N/Ti and F/Ti ratios determined by XPS after annealing. Second, the absorbance near 430 nm increases the most in the N−TiO_2 samples and the least in the fully fluorinated sample. There are several possible explanations for these results. On one hand, the samples fluorinated at pH ∼ 3 have transformed into the anatase phase and likely contain fewer defects. On the other hand, surface fluoride has been know to inhibit loss of nitrogen upon annealing.[59] These results also reveal an important point that is absent in many previous studies. In many prior reports, the appearance of the absorption peak at ∼430 nm after annealing samples was used as evidence for nitrogen "doping". On the basis of the XPS, we clearly have nitrogen, but the samples annealed to 100 °C have more nitrogen than the samples annealed to 400 °C; however, they do not show the peak near 430 nm. We favor the conclusion that the increase in absorbance is due to the creation of oxygen vacancies. The origin of the spectral changes in doped TiO_2 has been scrutinized by Kuznetsov and Serpone.[72] Specifically, they suggested that the enhanced visible absorption is due to the formation of F-type color centers. In order to determine if the increased absorption correlated with the increased visible light photoactivity, the decolorization of methylene blue was tested on these materials.

Figure 8 shows UV−vis spectra of methylene blue decolorization with the as-synthesized N−TiO_2 and F,N−TiO_2 nanoparticles (i.e., not annealed). The maximum peak for methylene blue is about 664 nm. The peak at 600 nm is due to a dimer. With prolonged irradiation, the peak shifts to a shorter wavelength, which indicates demethylation has occurred.[73−76] In general, the rate of methylene blue decolorization decreases one order of magnitude after the samples were annealed from 100 to 400 °C. Specifically, the first order rate constant for the decolorization of methylene blue drops from 1.6×10^{-2} min^{-1} to 2.0×10^{-3} min^{-1} for the F,N−TiO_2 samples after annealing at 100 and 400 °C, respectively. In addition, in control experiments with P25 TiO_2 as the photocatalyst, the rate constant of methylene blue decolorization was measured to be 6.2×10^{-4} min^{-1}. Over this temperature range, both the nitrogen and fluoride content decrease. To better understand the origin of photoactivity, three samples were irradiated simultaneously and subsequently analyzed with mass spectrometry to elucidate the decomposition pathway. Figure 9 shows mass spectra of methylene blue after irradiation for 210 min on the as-synthesized N−TiO_2, fully and partially fluorinated N−TiO_2. The latter samples were fluorinated at pH = 7. The molecular ion of methylene blue appears at 284 Da. Loss of the first methyl group yields Azure B at 270 Da; loss of the second methyl group yields Azure A at 256 Da, and loss of the third methyl group yields Azure C at 242 Da. The percent labeled in the spectra indicate the relative amount of each ion with respect to the base methylene blue peak. Clearly, demethylation occurs to a larger extent on the fully fluorinated nanoparticles.

CONCLUSIONS

Using a two-step synthesis method, nitrogen-doping and surface fluorination steps have been decoupled. The extent of fluorination can be controlled by the pH of the aging solution. At pH ∼ 3, the maximum amount of surface fluoride is adsorbed and the particles convert into the anatase phase. There is no evidence for bulk doping of fluoride. The fluorinated particles are thermally stable and less susceptible to sinter. Annealing the F,N−TiO_2 particles results in the loss of surface fluoride and nitrogen and a decrease in surface area. Irradiation of methylene blue with visible light in the presence of the N−TiO_2 and F,N−TiO_2 photocatalysts and subsequent product analysis by mass spectrometry, shows that the mechanism of decolorization is via demethylation. The visible light photoactivity is greatest when the surface fluoride concentration is at a maximum.

AUTHOR INFORMATION

Corresponding Author

*E-mail: gjs@ua.edu.

dx.doi.org/10.1021/jp5071049 | J. Phys. Chem. B XXXX, XXX, XXX−XXX

Present Address

[†]J.I.B.: The University of Oklahoma, 101 Stephenson Pkwy, Norman, OK 73019.

Notes

The authors declare no competing financial interest.

■ ACKNOWLEDGMENTS

The authors thank the National Science Foundation for support of this work through the NIRT Grant CTS-0608896. The authors thank the Central Analytical Facility at The University of Alabama for use of the Kratos XPS spectrometer, Dr. Tom Vaid for use of his DRS and XRD spectrometers, and Dr. Shane Street for use of his DRIFTS spectrometer. Finally we thank Andrew Guo for helping measure the point of zero charge and Alexandra Arnold for measuring the methylene blue decolorization.

■ REFERENCES

(1) Hu, X.; Li, G.; Yu, J. C. Design, Fabrication, and Modification of Nanostructures Semiconductor Materials for Environmental and Energy Applications. *Langmuir* **2010**, *26*, 3031−3039.

(2) Chen, X.; Liu, L.; Yu, P. Y.; Mao, S. S. Increasing Solar Absorption for Photocatalysis with Black Hydrogenated Titanium Dioxide Nanocrystals. *Science* **2011**, *331*, 746−749.

(3) Hoffmann, M. R.; Martin, S. T.; Choi, W.; Bahnemann, D. W. Environmental Applications of Semiconductor Photocatalysis. *Chem. Rev.* **1995**, *95*, 69−96.

(4) Liu, G.; Wang, L.; Yang, H. G.; Cheng, H.-M.; Lu, G. Q. Titantia-Based Photocatalysts: Crystal Growth, Doping and Heterostructuring. *J. Mater. Chem.* **2010**, *20*, 831−843.

(5) Herrmann, J.-M. Fundamentals and Misconceptions in Photocatalysis. *J. Photochem. Photobiol., A* **2010**, *216*, 85−93.

(6) Akpan, U. G.; Hameed, B. H. The Advancements in Sol-Gel Method of Doped-TiO_2 Photocatalysts. *Appl. Catal. A* **2010**, *375*, 1−11.

(7) Park, Y.; Park, Y.; Kim, W.; Choi, W. Surface Modification of TiO_2 Photocatalysts for Environmental Applications. *J. Photochem. Photobiol., C* **2013**, *15*, 1−20.

(8) Dozzi, M. V.; Selli, E. Doping TiO_2 with p-Block Elements: Effects on Photocatalytic Activity. *J. Photochem. Photobiol., C* **2013**, *14*, 13−28.

(9) Sato, S. Photocatalytic activity of NO_x-doped TiO_2 in the Visible Light Region. *Chem. Phys. Lett.* **1986**, *123*, 126−128.

(10) Asahi, R.; Morikawa, T.; Ohwaki, T.; Aoki, K.; Taga, Y. Visible-Light Photocatalysis in Nitrogen-Doped Titanium Oxides. *Science* **2001**, *293*, 269−271.

(11) Ryu, J.; Choi, W. Substrate-Specific Photoactivities of TiO_2 and Multiactivity Test for Water Treatment Application. *Environ. Sci. Technol.* **2008**, *42*, 294−300.

(12) Chen, X.; Mao, S. S. Titanium Dioxide Nanomaterials: Synthesis, Properties, Modification and Applications. *Chem. Rev.* **2007**, *107*, 2891−2959.

(13) Yang, H. G.; Sun, C. H.; Qiao, S. Z.; Zou, J.; Liu, G.; Smith, S. C.; Cheng, H. M.; Lu Anatase, G. Q. TiO_2 Single Crystals with a Large Percentage of Reactive Facets. *Nature* **2008**, *453*, 638−642.

(14) Han, X.; Kuang, Q.; Jin, M.; Xie, Z.; Zheng, L. Synthesis of Titania Nanosheets with a High Percentage of Exposed (001) Facets and Related Photocatalytic Propoerties. *J. Am. Chem. Soc.* **2009**, *131*, 3152−3153.

(15) Wen, C. Z.; Jiang, H. B.; Qiao, S. Z.; Yang, H. G.; Qing Lu, G. Synthesis of High-Reactive Facets Dominated Anatase TiO_2. *J. Mater. Chem.* **2011**, *21*, 7052−7061.

(16) Zhang, H.; Wang, Y.; Liu, P.; Han, Y.; Yao, X.; Zou, J.; Cheng, H.; Zhao, H. Anatase TiO_2 Crystal Facet Growth: Mechanistic Role of Hydrofluoric Acid and Photoelectocatalytic Activity. *ACS. Appl. Mater. Interfaces* **2011**, *3*, 2472−2478.

(17) Sakthivel, S.; Janczarek, M.; Kisch, H. Visible Light Activity and Photoelectrochemical Properties of Nitrogen-Doped TiO_2. *J. Phys. Chem. B* **2004**, *108*, 19384−19387.

(18) Belver, C.; Bellod, R.; Fuerte, A.; Fernandez-Garcia, M. Nitrogen-Containing TiO_2 Photocatalysts Part 1. Synthesis and Solid Characterization. *Appl. Catal., B* **2006**, *65*, 301−308.

(19) Belver, C.; Bellod, R.; Stewart, S. J.; Requejo, F. G.; Fernandez-Garcia, M. Nitrogen-Containing TiO_2 Photocatalysts Part 2. Photocatalytic Behavior Under Sunlight Excitation. *Appl. Catal., B* **2006**, *65*, 309−314.

(20) Zhao, Y.; Qiu, X.; Burda, C. The Effects of Sintering on the Photocatalytic Activity of N-Doped TiO_2 Nanoparticles. *Chem. Mater.* **2008**, *20*, 2629−2636.

(21) Di Valentin, C.; Pacchioni, G. Trends in Non-Metal Doping of Anatase TiO_2: B, C, N and F. *Catal. Today* **2013**, *206*, 12−18.

(22) Batzill, M.; Morales, E. H.; Diebold, U. Influence of Nitrogen Doping on the Defect Formation and Surface properties of TiO_2 Rutile and Anatase. *Phys. Rev. Lett.* **2006**, *96*, 026103(4).

(23) Chen, H.; Nambu, A.; Wen, W.; Graciani, J.; Zhong, Z.; Hanson, J. C.; Fujita, E.; Rodriguez, J. A. Reaction of NH_3 with Titania: N-Doping of the Oxide and TiN Formation. *J. Phys. Chem. C* **2007**, *111*, 1366−1372.

(24) Cheung, S. H.; Nachimuthu, P.; Joly, A. G.; Engelhard, M. H.; Bowman, M. K.; Chambers, S. A. N Incorporation and Electronic Structure in N-Doped TiO_2(110) Rutile. *Surf. Sci.* **2007**, *601*, 1754−1762.

(25) Kim, Y. K.; Park, S.; Kim, K.-J.; Kim, B. Photoemission Study of N-Doped TiO_2(110) with NH_3. *J. Phys. Chem. C* **2011**, *115*, 18618−18624.

(26) Chen, X. B.; Burda, C. Photoelectron Spectroscopic Investigation of Nitrogen-doped Titania Nanoparticles. *J. Phys. Chem. B* **2004**, *108*, 15446−15449.

(27) Sathish, M.; Viswanathan, B.; Viswanath, R. P.; Gopinath, C. S. Synthesis, Characterization, Electronic Structure, and Photocatalytic Activity of Nitrogen-Doped TiO2 Nanocatalyst. *Chem. Mater.* **2005**, *17*, 6349−6353.

(28) Chen, C.; Bai, H.; Chang, C. Effect of Plasma Processing Gas Composition on the Nitrogen-Doping Status and Visible Light Photocatalysis of TiO_2. *J. Phys. Chem. C* **2007**, *111*, 15228−15235.

(29) Livraghi, S.; Chierotti, M. R.; Giamello, E.; Magnacca, G.; Paganini, M. C.; Cappelletti, G.; Bianchi, C. L. Nitrogen-Doped Titanium Dioxide in Active Photocatalytic reactions with Visible Light: A Multi-Technique Characterization of Differently prepared Materials. *J. Phys. Chem. C* **2008**, *112*, 17244−17252.

(30) Zhang, Z.; Wang, X.; Long, J.; Gu, Q.; Ding, Z.; Fu, X. Nitrogen-Doped Titanium Dioxide Visible Light Photocatalyst: Spectroscopic Identification of Photoactive Centers. *J. Catal.* **2010**, *276*, 201−214.

(31) Oropenza, F. E.; Marmer, J.; Egdell, R. G.; Palgrave, R. G. A Critical Evaluation of the Mode of Incorporation of Nitrogen in Doped Anatase Photocatalysyts. *Phys. Chem. Chem. Phys.* **2010**, *12*, 960−969.

(32) Livraghi, S.; Paganini, M. C.; Giamello, E.; Selloni, A.; Di Valevtin, C.; Pacchioni, G. Origin of Photoactivity of Nitrogen-Doped Titanium Dioxide under Visible Light. *J. Am. Chem. Soc.* **2006**, *128*, 15666−15671.

(33) Di Valentin, C.; Pacchioni, G.; Selloni, A.; Livraghi, S.; Giamello, E. Characterization of Paramagnetic Species in N-Doped TiO_2 Powders by EPR Spectroscopy and DFT Calculations. *J. Phys. Chem. B* **2005**, *109*, 11414−11419.

(34) Reyes-Garcia, E. A.; Sun, Y.; Reyes-Gil, K.; Raftery, D. ^{15}N Solid State NMR and EPR Characterization of N-Doped TiO_2 Photocatalysts. *J. Phys. Chem. C* **2007**, *111*, 14579−14588.

(35) DArienzo, M.; Scotti, R.; Wahba, L.; Battocchio, C.; Bemporad, E.; Nale, A.; Morazzoni, F. Hydrothermal N-Doped TiO_2: Explaining Photocatalytic Properties by Electronic and Magnetic Identification of N Active Sites. *Appl. Catal., B* **2009**, *93*, 149−155.

(36) Barolo, G.; Livraghi, S.; Chiesa, M.; Paganini, M. C.; Giamello, E. Mechanism of the Photoactivity Under Visible Light of N-Doped

Titanium Dioxide. Charge Carriers Migration in Irradiated N-TiO_2 Investigated by Electron Paramagnetic Resonance. *J. Phys. Chem. C* **2012**, *116*, 20887−20894.
(37) Di Valentin, C.; Finazzi, E.; Pacchioni, G.; Selloni, A.; Livraghi, S.; Czoska, A. M.; Chiesa, M.; Paganini, M. C.; Giamello, E. Density Functional Theory and Electron Paramagnetic Resonance Study on the Effect of N-F codoping of TiO_2. *Chem. Mater.* **2008**, *20*, 3706−3714.
(38) Dozzi, M. V.; Ohtani, B.; Selli, E. Absorption and Action Spectra Analysis of Ammonium Fluoride-Doped Titania Photocatalysts. *Phys. Chem. Chem. Phys.* **2011**, *13*, 18217−18227.
(39) Minero, C.; Mariella, G.; Maurino, V.; Vione, D.; Pelizzetti, E. Photocatalytic Transformation of Organic Compounds in the Presence of Inorganic Anions. 1. Hydroxyl-Mediated and Direct Electron-Transfer Reactions of Phenol on a Titanium Dioxide Fluoride System. *Langmuir* **2000**, *16*, 2632−2641.
(40) Minero, C.; Mariella, G.; Maurino, V.; Vione, D.; Pelizzetti, E. Photocataltic Transformations of Organic Compounds in the Presence of Inorganic Ions 2. Competetive Reactions of Phenol and Alcohols an a Titanium-Fluoride System. *Langmuir* **2000**, *16*, 8964−8972.
(41) Yu, J. C.; Yu, J.; Ho, W.; Jiang, Z.; Zhang, L. Effects of F-Doping on the Photocatalytic Activity and Microstructure of Nanocrystalline TiO_2 Powders. *Chem. Mater.* **2002**, *14*, 3808−3816.
(42) Vohra, M. S.; Kim, S.; Choi, W. Effects of Surface Fluorination on TiO_2 on the Photocatalytic Degradation of Tetramethylammonium. *J. Photochem. Photobiol., A* **2003**, *160*, 55−60.
(43) Yu, J.-G.; Yu, J. C.; Cheng, B.; Hark, S. K.; Iu, K. The Effect of F-Doping and Temperature on the Structural and Textural Evolution of Mesoporous TiO_2 Powders. *J. Solid State Chem.* **2003**, *174*, 372−380.
(44) Park, H.; Choi J, W. Effects of TiO_2 Surface Fluorination on the Photocatalytic Reactions and Photoelectrochemical Behaviors. *J. Phys. Chem. B* **2004**, *108*, 4086−4093.
(45) Mrowetz, M.; Selli, E. Enhanced Photocatalytic Formation of Hydroxyl Radicals on Fluorinated TiO_2. *Phys. Chem. Chem. Phys.* **2005**, *7*, 1100−1102.
(46) Xu, Y.; Lv, K.; Xiong, Z.; Leng, W.; Du, W.; Liu, D.; Xue, X. Rate Enhancement and Rate Inhibition of Phenol Degradation over Irradiated Anatase and Rutile TiO_2 on the Addition of NaF: New Insight into the Mechanism. *J. Phys. Chem. C* **2007**, *111*, 19024−19032.
(47) Wang, Q.; Chen, C.; Zhao, D.; Ma, W.; Zhao, J. Change of Adsorption Modes of Dyes on Fluorinated TiO_2 and its Effect of Photocatalytic Degradation of Dyes Under Visible Irradiation. *Langmuir* **2008**, *24*, 7338−7345.
(48) Kim, J.; Choi, W.; Park, H. Effects of TiO_2 Surface Fluorination on Photocatalytic Degradation of Methylene Blue and Humic Acid. *Res. Chem. Intermed.* **2010**, *36*, 127−140.
(49) Minella, M.; Faga, M. G.; Maurino, V.; Minero, C.; Pelizzetti, E.; Coluccia, S.; Martra, G. Effect of Fluorination on the Surface Properties of Titania P25 Powder: An FTIR Study. *Langmuir* **2009**, *26*, 2521−2527.
(50) Dozzi, M. V.; Selli, E. Effects of Phase Composition and Surface Area on the Photocatalytic Paths on Fluorinated Titania. *Catal. Today* **2013**, *206*, 26−31.
(51) Mrowetz, M.; Selli, E. Enhanced Photocatalytic Formation of Hydroxyl Radicals on Fluorinated TiO_2. *Phys. Chem. Chem. Phys.* **2005**, *7*, 1100−1102.
(52) Li, D.; Haneda, H.; Hishita, S.; Ohashi, N. Visible-Light-Driven N-F-Codoped TiO_2 Photocatalysts. 1. Synthesis by Spray Pyrolysis and Surface Characterization. *Chem. Mater.* **2005**, *17*, 2588−2595.
(53) Li, D.; Haneda, H.; Hishita, S.; Ohashi, N. Visible-Light-Driven N-F-Codoped TiO_2 Photocatalysts. 2. Optical Characterization, Photocatalysis, and Potential Application to Air Purification. *Chem. Mater.* **2005**, *17*, 2596−2602.
(54) Li, D.; Ohashi, N.; Hishita, S.; Kolodiazhnyi, T.; Heneda, H. Origin of Visible-Light-Driven Photocatalysis: A Comparative Study on N/F-Doped and N-F-Codoped TiO_2 Powders by Means of Experimental Characterizations and Theoretical Calculations. *J. Solid State Chem.* **2005**, *178*, 3293−3302.
(55) Huang, D.-G.; Liao, S.-J.; Liu, J.-M.; Dang, Z.; Petrik, L. Preparation of Visible-Light Responsive N-F−codoped TiO_2 Photocatalysts by a Sol-Gel Solvothermal Method. *J. Photochem. Photobiol., A* **2006**, *184*, 282−288.
(56) Wang, Q.; Chen, C.; Ma, W.; Zhu, H.; Zhao, J. Pivotal Role of Fluorine in Tuning Band Structure and Visible Photocatalytic Activity of Nitrogen-Doped TiO_2. *Chem.—Eur. J.* **2009**, *15*, 4765−4769.
(57) Livraghi, S.; Elghniji, K.; Czoska, A. M.; Paganinia, M. C.; Giamelloa, E.; Ksibi, M. Nitrogen-Doped and Nitrogen-Fluorine-Codoped Titanium Dioxide, Nature and Concentration of the Photoactive Species and Their Role in Determining the Photocatalytic Activity Under Visible Light. *J. Photochem. Photobiol., A* **2009**, *205*, 93−97.
(58) Meng, Y.; Chen, J.; Wang, Y.; Dingy, H.; Shan, Y. (N,F)−Codoped TiO_2 Nanocrystals as Visible Light-Activated Photocatalysts. *J. Mater. Sci. Technol. (Shenyang, China)* **2009**, *25*, 73−76.
(59) Liu, S.; Yu, J.; Wang, W. Phys. Chem. Chem. Phys. Effects of Annealing on the Microstructure and Photoactivity of Fluorinated N-doped TiO_2. *Phys. Chem. Chem. Phys.* **2010**, *12*, 12308−12315.
(60) Wu, G.; Wen, J.; Nigro, S.; Chen, A. One-step Synthesis of N- and F-codoped Mesoporous TiO_2 Photocatalysts with High Visible Light Activity. *Nanotechnology* **2010**, *21*, 085701(6).
(61) He, Z.; Que, W.; Chen, J.; Yin, X.; He, Y.; Ren, J. Photocatalytic Degradation of Methyl Orange over Nitrogen-Fluorine Codoped TiO_2 Nanobelts Prepared by Solvothermal Synthesis. *ACS Appl. Mater. Interfaces* **2012**, *4*, 6816−6826.
(62) Hamilto, J. W. J.; Byrne, J. A.; Dunlop, P. S. M.; Dionysious, D. D.; Palaez, M.; O'Shea, K.; Synnott, D.; Plillai, S. C. Evaluating the Mechanism of Visible-Light Activity for N,F-TiO_2 Using Photoelectrochemistry. *J. Phys. Chem. C* **2014**, *118*, 12206−112215.
(63) Schulthess, C. P.; Sparks, D. L. Back Titration Technique for Proton Isotherm Modeling of Oxide Surfaces. *Soil Sci. Soc. Am. J.* **1986**, *50*, 1405−1411.
(64) Baltrusaitis, J.; Jayaweera, P. M.; Grassian, V. H. XPS Study of Nitrogen Dioxide Adsorption on Metal Oxide Particle Surfaces Under Different Environmental Conditions. *Phys. Chem. Chem. Phys.* **2009**, *11*, 8295−8305.
(65) Kosmulski, M. The Significance of the Difference in the Point of Zero Charge Between Anatase and Rutile. *Adv. Colloid Interface Sci.* **2002**, *99*, 255−264.
(66) Liao, L.-F.; Lien, C.-F.; Shieh, D.-L.; Chen, M.-T.; Lim, J.-L. FTIR Study of Adsorption and Photoassisted Oxygen Isotopic Exchange of Carbon Monoxide, Carbon Dioxide, Carbonate, and Formate on TiO_2. *J. Phys. Chem. B* **2002**, *106*, 11240−11245.
(67) Su, W.; Zhang, J.; Feng, Z.; Chen, T.; Ying, P.; Li, C. Surfaces Phases of TiO_2 Nanoparticles Studies by UV Raman and FT-IR Spectroscopy. *J. Phys. Chem. C* **2008**, *112*, 7710−7716.
(68) Panayotov, D. A.; Yates, J. T., Jr. Depletion of Conduction Band Electrons in TiO_2 by Water Chemisorption: IR Spectroscopic Studies of the Independence of Ti-OH Frequencies on Electron Concentration. *Chem. Phys. Lett.* **2005**, *410*, 11−17.
(69) Minella, M.; Faga, M. G.; Maurino, V.; Minero, C.; Pelizzetti, E.; Colucccia, S.; Martra, G. Effects of Fluorination on the Surface Properties of Titania P25 Powder: FTIR Study. *Langmuir* **2010**, *26*, 2521−2527.
(70) Ohno, T.; Koji, K.; Matsumura, M. Photocatalytic Activities of Pure Rutile Particles Isolated from TiO_2 Powder by Dissolving the Anatase Component in HF Solution. *J. Phys. Chem. B* **2001**, *105*, 2417−2420.
(71) Lv, K. L.; Xiang, Q. J.; Yu, J. G. Effect of Calcination Temperature on Morphology and Photocatalytic Activity of Anatase TiO_2 Nanosheets with Exposed {001} Facets. *Appl. Catal., B* **2011**, *104*, 275−281.
(72) Kuznetsov, V. N.; Serpone, N. On the Origin of the Spectral Bands in the Visible Absorption Spectra of Visible-Light-Active TiO_2 Specimens Analysis and Assignments. *J. Phys. Chem. C* **2009**, *113*, 15110−15123.

(73) Zhang, T.; Oyama, T.; Aoshima, A.; Hidaka, H.; Zhao, J.; Serpone, N. Photooxidative N-demethylation of Methylene Blue in Aqueous TiO_2 Dispersions Under UV Irradiation. *J. Photochem. Photobiol., A* **2001**, *140*, 163−172.
(74) Houas, A.; Lachheb, H.; Ksibi, M.; Elaloui, E.; Guillard, C.; Herrmann, J.-M. Photocatalytic. Degradation Pathway of Methylene Blue in Water. *Appl. Catal., B* **2001**, *31*, 145−157.
(75) Yan, X.; Ohno, T.; Nishijima, K.; Abe, R.; Ohtani, B. Is Methylene Blue an Appropriate Substrate for a Photocatalytic Activity Test? A Study with Visible-Light Responsive Titania. *Chem. Phys. Lett.* **2006**, *429*, 606−610.
(76) Yu, Z.; Chuang, S. S. C. Probing Methylene Blue Photocatalytic Degradation by Adsorbed Ethanol with In Situ IR. *J. Phys. Chem. C* **2007**, *111*, 13813−13820.